ABSTRACT

JAYANTHI SURYANARAYANAN. Design and Fabrication of Toroidal Inductors for Mixed Signal Packaging. (Under the direction of Dr.Michael B. Steer.)

The demand for efficient, lightweight consumer products created the need for miniaturization of passive components especially inductors which are some of the bulkiest parts of an integrated system. The purpose of the work described here was to study toroidal inductor structures since they were compact and self-shielding. Toroidal inductors were modeled using a commercial electromagnetic simulator. The results show that these structures have good characteristics in terms of inductance, quality factor and area. Three different structures are fabricated and experimentally characterized using the HP Vector Network Analyzer. We also make several observations about the effect of the placement of each pair of top and bottom metal strips with respect to each other on the flux linkage and hence, the inductance and quality factor of the inductor.

DESIGN AND FABRICATION OF TOROIDAL INDUCTORS FOR MIXED SIGNAL PACKAGING

by

Jayanthi Suryanarayanan

A thesis submitted to the Graduate Faculty of
North Carolina State University
in partial fulfillment of the
requirements for the Degree of
Master of Science

Electrical Engineering

Raleigh

December 2002

APPROVED BY:

Chair of Advisory Committee

DEDICATION

I dedicate this thesis to my parents for always being there for me and supporting me in everything I do.

BIOGRAPHY

Jayanthi Suryanarayanan was born in Tanjore, India in 1978. She grew up in Bombay, where she also got her Bachelors in Electronics Engineering from Bombay University in 2000. After working for a year as Systems engineer in Wipro Ericsson, she joined NC State in Fall 2001 for the Masters program in Electrical Engineering.

ACKNOWLEDGEMENTS

I take this opportunity to thank all those people who offered me their greatest support in completing my Masters here at North Carolina State University.

I would first like to thank my advisor, Professor Michael Steer for his support and guidance in completing my graduate studies and research work. He has been an excellent guide and the passion with which he works is truly impressive. I have thoroughly enjoyed the learning experience this past year and I am glad I got the opportunity to work with him. I would also like to thank Dr. Douglas Barlage and Dr. Paul Franzon for serving on my advisory committee and for their valuable suggestions.

I also take this opportunity to thank everybody who helped me in every way in completing this thesis. The list is long but I'll name them anyway. I have to thank Jayesh Nath, Steve Lipa and Mark Buff for helping me so much in completing my thesis. I specially thank Keyoor Gosalia for making those structures so patiently. I could not have done it without his skill and effort. Thanks to Sonali, Rachana and Aditya for all the necessary diversions and good lunch breaks.

My parents deserve the biggest share in my success, and I thank them for having faith in me and always stressing on the importance of education. Thanks Mom for those long phone calls. Thanks Dad for everything. You are the reason I am here.

Contents

List of Figures

Chapter 1

Introduction

1.1 Background

There has been a large demand for passive components for consumer products like pagers and cellular phones leading to a lot of work to improve passive component fabrication and packaging. One of the main uses of inductors is in transistor biasing networks, for instance as RF coils to short circuit the device to DC voltage conditions.

One of the major issues in passive component fabrication has been the fabrication of three-dimensional inductors on silicon and in mixed signal package, and their miniaturization. The miniaturization technology of inductors is much less advanced compared to other passive components (e.g. resistors and capacitors), greatly limiting the integration of electromagnetic devices.

Inductors, in general, occupy a lot of area on the chip since large magnetic cross sectional areas are required to obtain good inductance and Q-factor. This obviously affects any attempts at miniaturization. There is a major attempt to take the inductor or a huge portion of it off-chip and into the package.

In general, planar spiral inductors are fabricated in integrated circuits, the spiral inductor being the dominant choice since it is a planar inductor and hence easy to fabricate using two dimensional techniques. In integrated systems it is difficult to achieve high Q and high inductance partly due to the geometry of the spiral inductor and partly due to the finite conductivity of the silicon substrate on which the inductor

is fabricated.

1.2 Motivation

The issues we are trying to address when fabricating integrated inductors are maximizing Q, maximizing inductance, increasing the self-resonant frequency, reducing the area occupied by the inductor and making them mechanically robust. The entire motivation behind this research has been trying to address these issues especially in trying to make the inductor more compact, at the same time, offering much higher inductance than the spiral or solenoid inductors which are currently the popular inductors used in integrated systems. This would lead to smaller, lighter, more efficient components being used in consumer products.

1.3 Organization of Thesis

Chapter 2 is a literature review of the inductor, the types of inductors fabricated in integrated systems and the issues involved in fabrication and miniaturization. In Chapter 3, the working and analysis of the toroidal inductor is presented. Chapter 4 describes the simulations and experiments performed to realize the toroidal inductor structure and the results obtained from simulations done using HFSS and measurements made on fabricated structures. Chapter 5 presents the conclusions and describes future work.

Chapter 2

Literature Review

2.1 Classic Model of an Inductor

An inductor is basically a wire coiled in such a way as to increase the magnetic flux linkage between the turns of the coil. This increases the self-inductance of the wire beyond what it would have been without flux linkage.

An ideal inductor is characterized by a purely reactive impedance ($Z = jX_L$) which is proportional to the inductance only. The phase of the signal across the ideal inductor would always be +90 degrees out of phase with the applied voltage and there would be no effect of DC current bias on its behavior.

Figure 2.1 shows what the inductor coil looks like at RF frequencies. The equiv-

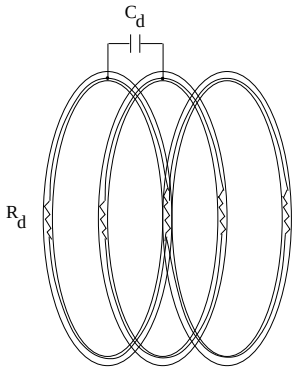

Figure 2.1: Distributed capacitance and series resistance in the inductor.

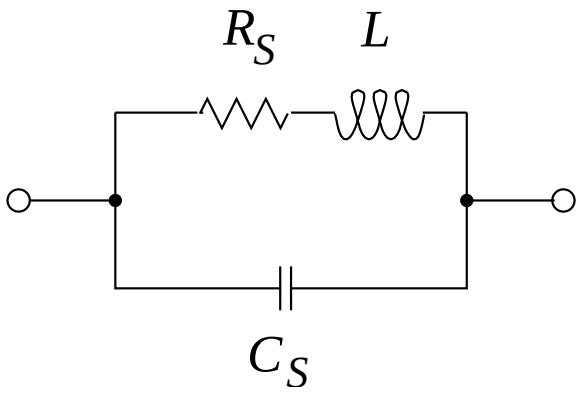

Figure 2.2: Equivalent circuit model of an inductor coil at high frequencies.

alent circuit model of the inductor is shown in Figure 3.4.

Since the windings are adjacently positioned a minute voltage drop occurs between adjacent turns giving rise to a parasitic capacitance effect. This effect is called the *d*istributed capacitance $\mathbf{C_d}$. The parasitic shunt capacitance C_s and the series resistance R_s represent composite effects of distributed capacitance C_d and resistance R_d respectively in the inductor coil as shown in Figure 3.4. When circuits are comparable in size to the wavelength, effects are distributed rather than lumped and the electric energy storage in parts of a primarily inductive element or the magnetic energy storage in parts of a primarily capacitive element becomes important. In the present case there is electric field (capacitive) coupling between the turns of the inductor. A good way to represent this effect is to add a capacitive element between each pair of adjacent turns. At high frequencies the effect of these capacitors is to bypass some of the turns so that not all turns have the same current.

So in a real inductor the distributed capacitance C_d affects the reactance of the inductor. Initially, at lower frequencies, the inductor's reactance parallels that of an ideal inductor. However the reactance deviates from the ideal curve and increases at a much faster rate until it reaches a peak at the inductor's *s*elf-resonant frequency (SRF). The SRF is given by $SRF = 1/2\pi\sqrt{LC_s}$. As the frequency continues to increase the distributed capacitance C_d becomes dominant. So the inductor's reactance begins to decrease with frequency, a voltage phase shift of -90 degrees is observed and

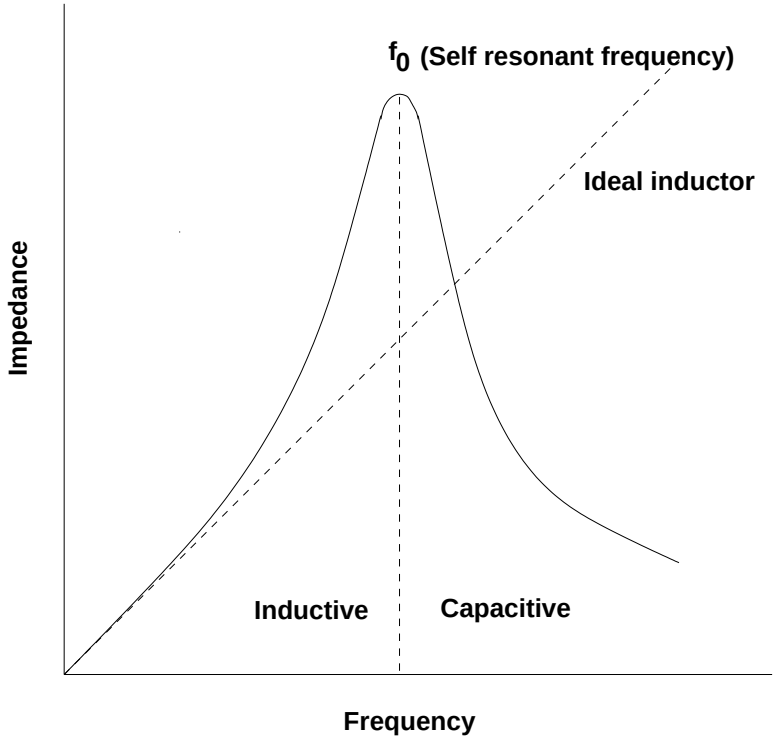

Figure 2.3: Frequency response of the impedance of an ideal inductor and a practical inductor.

the inductor begins to look like a capacitor. This behavior of the inductor is shown in Figure 2.3.

Theoretically the resonance peak would occur at infinite reactance. However, due to the series resistance of the coil, some finite impedance is seen at resonance. The series resistance also serves to broaden the resonance peak of the impedance curve of the coil. To characterize the impact of the series resistance the *q*uality factor Q is commonly used. The Q is the ratio of an inductor's reactance to its series resistance ($Q = X_L/R$) and characterizes the resistive loss in the inductor. For tuning purposes, this ratio should be as high as possible. If the coil were a perfect conductor, its Q would be infinite and the inductor would be lossless. But since there is no perfect conductor an inductor always has a finite Q.

At low frequencies, the Q factor is very good because the only resistance seen is the dc resistance of the wire which is very small. But as the frequency increases, *s*kin

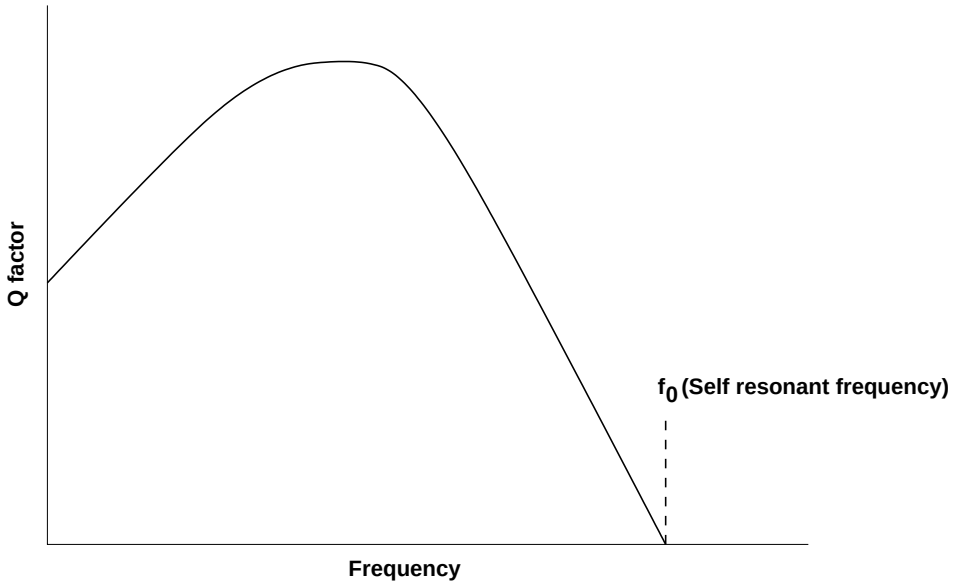

Figure 2.4: Change in Q factor with frequency

effect [1] and winding capacitance begin to degrade the quality of the inductor. At low frequencies, Q will increase directly with frequency because its reactance is increasing and skin effect has not yet become noticeable. Soon however the skin effect becomes factor with the Q rising but a lower rate and we get a gradually decreasing slope in the curve. The change in the Q of an inductor with frequency is shown in Figure 2.4.

The flat portion of the curve occurs because the series resistance and the reactance are changing at the same rate. As the frequency increases beyond this point, the winding capacitance and skin effect of the windings combine to decrease the Q of the inductor to zero at its self-resonant frequency.

[1] Skin effect is characterized by skin depth, $\delta = 1/\sqrt{f\pi\mu\sigma}$ where μ is the permeability and σ is the conductivity of the metal

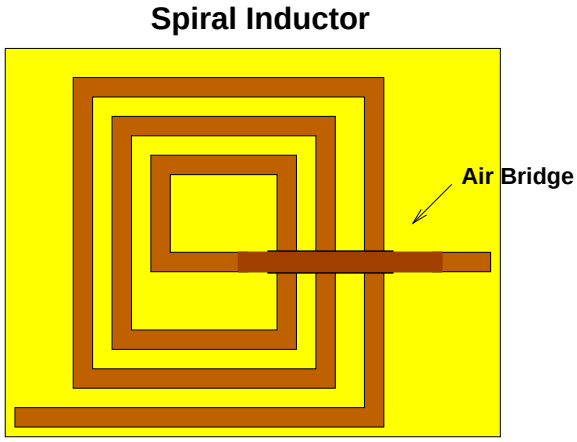

Figure 2.5: An on-chip spiral inductor.

2.2 Comparison of Inductors Fabricated in Integrated Systems

Integrated inductors are typically formed on-chip or embedded in the chip package or board. Now the three-dimensional nature of an inductor makes it difficult to fabricate it in an IC using conventional two dimensional fabrication techniques. In general, spiral or solenoid-type inductors are fabricated in integrated circuits, the spiral inductor being the dominant choice since it is a planar inductor and hence easy to fabricate using two dimensional techniques. A common type of on-chip spiral inductor is shown in Figure 2.5. This is contrary to macro-inductor structures which are typically solenoidal or toroidal. In integrated systems it is difficult to achieve high Q and high inductance partly due to the geometry of the spiral inductor and partly due to the finite conductivity of the silicon substrate on which the inductor is fabricated. Another major issue in fabricating an on-chip inductor is that it takes up a lot of real estate. Inductors up to 10 nH can be fabricated on-chip. Beyond this it is better to have either the entire inductor or a majority of it off-chip as a part of the RFIC package.

One of the major sources of loss for inductors on silicon is substrate loss due to the finite conductivity of the substrate and the resulting current flow. These induced

currents follow a path under the conductors of the spiral and, just as with ground plane eddy currents, lower the inductance achieved. Eddy currents are also excited in the metal backing of dies or package metallization.

Most silicon substrates are at least slightly doped, usually of p-type. With heavily doped n-type strips arranged radially from the center axis of the spiral, the eddy currents are blocked. They achieved an increase of the Q from 5.3 to 6.0 at 3.5 GHz and from 4.3 to 4.5 at 2.0 GHz. In the spiral inductor model, the effect was also to reduce the shunt resistance and capacitance to the substrate.

Parasitic capacitance results in resonance of the on-chip inductance structure and hence the frequency of operation. With GaAs ($\varepsilon_r = 12.85$) the effective permittivity of the medium can be reduced by adding a polyimide layer ($\varepsilon_r = 3.2$) and using metallization on top of this layer [14]. Thus, the capacitance is substantially reduced. This is at the cost of poorer thermal management as the thermal conductivity of polyimide is substantially lower (about 100 times) than that of GaAs, and so the power handling capability is compromised. Coupling this with thicker metallization to reduce resistance can result in a Q that is 50% larger and a self-resonant frequency that is 25% higher [14].

We now return to the issue of the finite conductivity of the silicon substrate. The inducement of charges in the silicon and the insignificant skin depth of the silicon substrate has the effect of increasing the capacitance of an interconnect line over silicon as the electric field lines are terminated on the substrate charges. (This effect is in addition to the induction of eddy currents in the substrate as discussed earlier.) Now the magnetic field lines penetrate some distance into the substrate so that the LC product is greater than if the substrate was insulating (as with GaAs). The effect is that the velocity of propagation along the interconnect ($= 1/\sqrt{LC}$) is reduced, leading to what is called the slow wave effect. This means that very small inductances can be realized using short lengths of interconnect arranged so that fields, particularly the magnetic field, penetrates the substrate. This effect can be adequately simulated using planar electromagnetic simulators that allow the conductivity of media to be specified. Simulation is necessary as the effect is a complex function of geometry and substrate conductivity, and generalizations available for use in design are not

available.

The lowest loss inductors are obtained by etching away the underlying substrate or by using insulating or very high resistivity bulk material. Loss is also reduced by separating the planar inductor from the ground plane and additional dielectric layers have been deposited on a chip to achieve this. Volant and Groves [15] obtained a Q of 18 at 10 GHz with a 4 μm thick aluminum-copper spiral inductor using this approach. When all steps have been taken then the dominant loss mechanism is current crowding [16]. This is a particular problem with multi-turn spiral inductors which are required to realize high inductance values. Current crowding results when the magnetic field of one turn penetrates an adjacent trace creating eddy currents so that current peaks on the inside edge of the victim trace (towards the center of the spiral) and reduces on the outside edge. This constricts current and results in higher resistance than would be predicted from skin effect and DC resistance alone [16]. The key requirement then is that magnetic flux be confined while still achieving flux linkage. The proposed toroidal inductor does just this.

Planar inductors are often fabricated in close proximity to each other. The coupling of adjacent planar inductors depends on the separation of the inductors, shielding, geometry and the resistivity of the underlying substrate. An effective measure of shielding is to use a discontinuous guard ring [17]. This however reduces the originally designed inductance values because of the image currents induced in the ring [18].

In summary the best that can be achieved for conventional spiral inductors on low resistivity silicon is around 20.

The issues we are trying to address when fabricating integrated inductors are:

- Maximizing Q,
- maximizing inductance,
- increasing the self-resonant frequency and
- reducing area occupied by the inductor.

The most severe problem that degrades Q factor at high frequencies (above 500MHz) is the I^2R losses from eddy currents in the metal traces that make up the spiral induc-

tor. The spiral's B-field generated by nearby turns passes perpendicularly through the traces, setting up eddy currents and pushing currents to the trace edges. The result is a quadratic increase in resistance with frequency with the frequency decided by the trace width, pitch and sheet resistance. The problem is not reduced by using traces of lower resistance either.

Fields produced by the spiral inductor penetrate the substrate and as a ground plane is located at a relatively short distance, the eddy currents on the ground plane reduce the inductance that would otherwise be obtained. The eddy current in the ground conductor rotates in a direction opposite to that of the spiral itself. Consequently the inductance of the image inductor in the ground is in the opposite direction to that produced by the spiral itself, with the consequent effect that the effective total inductance is reduced.

Since the spiral inductor requires a lead wire to connect from the inside end of the coil to the outside a capacitance is introduced between the conductor and the lead wire. This is one of the dominant stray capacitances of the spiral inductor and it serves to reduce the self-resonant frequency of the inductor.

The spiral inductor takes up large two-dimensional spaces compared to other inductor types with the same number of turns. Also the direction of flux of the spiral inductor is perpendicular to the substrate which can cause more interference with underlying circuitry or other vertically integrated passives.

Though the solenoid-type inductor has better electrical properties (high Q and high inductance) and is more compact than the spiral inductor it has its problems. These can be discussed in comparison with the toroidal inductor.

The air-core solenoidal inductor requires more number of turns than the toroidal inductor for a given inductance. So there is more ac resistance in a solenoid compared to the toroid which reduces its Q factor at a given frequency.

In a typical air core inductor, the magnetic flux lines linking the turns of the inductor take the shape shown in Figure 2.6.

The air surrounding the inductor is definitely part of the magnetic-flux path. So the solenoid tends to radiate RF signals flowing within. To reduce radiation the inductor has to be surrounded by a bulky shield which tends to reduce available

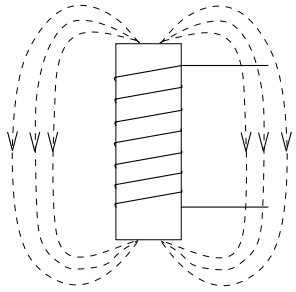

Figure 2.6: Solenoid-type inductor

space and the Q of the inductor it is shielding. On the other hand a toroid completely contains the magnetic flux within the material itself thus preventing RF signals from radiating. Practically some minimal radiation occurs. But bulky shields are not required surrounding the inductor.

Chapter 3

Toroidal Inductor

3.1 Introduction

Having explained the advantages of toroidal inductors over other types of inductors fabricated on silicon this chapter discusses the theory behind the proposed inductor. The inductor is also analyzed for turns of rectangular cross section.

3.2 Theory

If a long solenoid is bent into a circle and closed on itself, a toroidal coil, or toroid, is obtained as shown in Figure 3.1. When the toroid has a uniform winding of many turns, the magnetic lines of flux are almost entirely confined to the interior of the winding, B being substantially zero outside. If the ratio R/r is large, one may calculate B as though the toroid were straightened out into a solenoid.

The magnetic lines of flux produced by a current in a toroidal coil form closed loops. Each line that passes through the entire toroid links the current N times. This is shown in Figure 3.2. If all the lines link all the turns, the total magnetic flux linkage Λ of the toroid is equal to the total magnetic flux ψ_m through the toroid times the number of turns.

$$\Lambda = N\psi_m. \tag{3.1}$$

The unit of flux linkage is Wbturns.

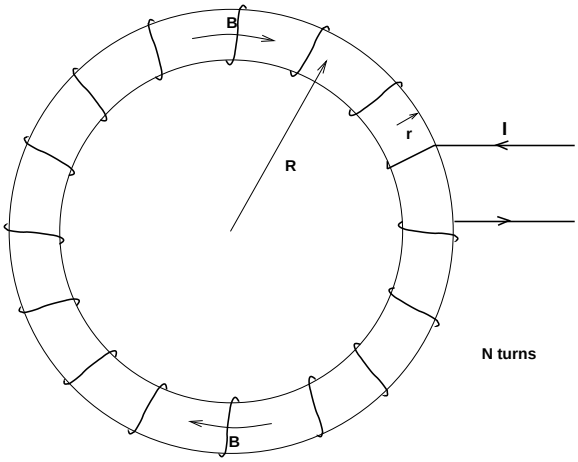

Figure 3.1: Toroidal inductor

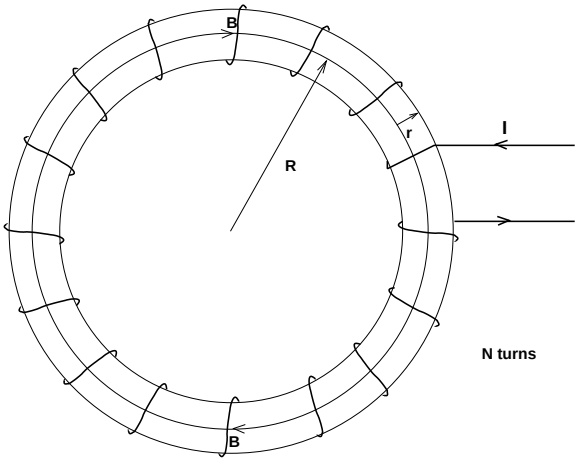

Figure 3.2: Toroidal inductor and magnetic flux lines

Thus, the magnetic flux linkage is

$$\Lambda = N\psi_m = NBA = N\frac{\mu NI}{2\pi R}\pi r^2 = \frac{\mu N^2 I \pi r^2}{2\pi R} = \frac{\mu N^2 r^2 I}{2R}. \tag{3.2}$$

By definition the inductance L is the ratio of the total magnetic flux linkage to the current I through the inductor.

$$L = \frac{N\psi_m}{I} = \frac{\Lambda}{I}. \tag{3.3}$$

This definition is satisfactory for a medium of constant permeability. Inductance has the dimensions of magnetic flux (linkage) divided by current.

The inductance of the toroid is then

$$L = \frac{\Lambda}{I} = \frac{\mu N^2 r^2}{2R}. \tag{3.4}$$

where, L = inductance of toroid, H

μ = permeability (uniform and constant) of medium inside coil, Hm^{-1}

N = number of turns of toroid, dimensionless

r = radius of coil, m

R = mean radius of toroid, m.

At higher frequencies, when turns are relatively close together current elements in neighboring turns will be near enough to produce nearly as much effect upon current distribution in a given turn as the current in that turn itself. The separation between internal and external inductance that is done at low frequencies to take into consideration the cross section of the wire (provided it is small compared to the loop radius r) in the expression for the internal inductance may not be possible for these coils because a given field line may be sometimes inside and sometimes outside of the conductor. Distributed capacitance is also an important issue at high frequencies as explained before.

3.3 Analysis

Designing the toroidal inductor with turns of rectangular cross section

The isometric view of the toroidal inductor structure as simulated on HFSS is shown in Figure 3.3.

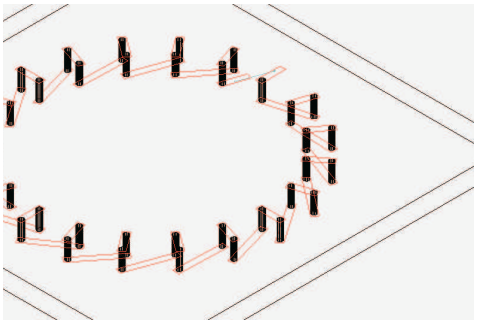

Figure 3.3: Toroid-type inductor structure as simulated on HFSS.

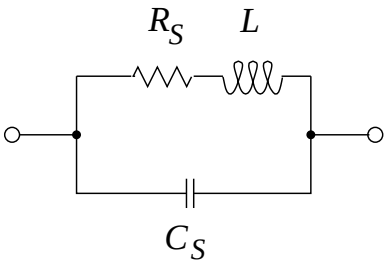

Figure 3.4: Equivalent circuit model of an inductor coil at high frequencies.

The equivalent circuit of the high frequency toroidal inductor is as shown in Figure 3.4.

Since the inductor is being designed to operate in the range of 100 MHz to 1 GHz the design of the toroidal inductor for an impedance of 50 Ω at 100 MHz is done here as an example. For an impedance of $X_L = 50\ \Omega$ and frequency $f = 100$ 1MHz the inductance is found to be around 80 nH.

Inductance of a toroidal inductor structure is:

$$L = \frac{\mu_o \mu_r N^2 A_c}{l_c} \tag{3.5}$$

where, A_c is the cross sectional area of the winding and l_c is the mean length of the toroid. This implies that the inductance L is proportional to the square of the number of turns (N^2) keeping the remaining parameters constant. Clearly increasing the number of turns increases the inductance but there is also a winding capacitance associated which increases as the inductor turns come close together. The effect of this capacitance is given by the shunt capacitance C_s shown in Figure 3.4.

The distributed capacitance resonates out the inductance of the toroid at a particular self-resonant frequency. At this frequency, the Q of the inductor drops to zero ideally as the impedance approaches infinity. To approximate the effect of the capacitance C_s, the formula of an ideal parallel-plate capacitor as given in Equation 3.6 is used.

$$C_s = \epsilon_o \epsilon_r A/d \tag{3.6}$$

In our case the separation d between the plates is assumed to be equal to the distance between the turns. Therefore

$$d = l/N = 2\pi R/N \tag{3.7}$$

where,
l is the length of the toroid and
R is the mean radius of the toroid. The area can be estimated as

$$A = 2(w_c \ + h_c \ )d \ N \tag{3.8}$$

where
w_c is the width of the metal strip,
h_c is the height of the via,
d is the diameter of the via, and
N is the number of turns of the inductor. So it can be concluded that

$$C_s = \epsilon_o \epsilon_r [2(w_c + h_c)d] N^2 / 2\pi R. \tag{3.9}$$

For a 20 turn inductor with $w_c = 50$ μm, $h_c = 250$ μm and diameter of via, $d = 20$ μm and assuming the dielectric constant of the substrate to be $\epsilon_r = 3.2$ the distributed capacitance is found to be $C_s = 17.31$ fF.

So the self-resonant frequency, f_o of the structure is given by

$$f_o = \frac{1}{2\pi\sqrt{LC}}. \tag{3.10}$$

The self-resonant frequency has to be higher than the operating frequency of the structure so that the inductor has a band of frequencies in which it can be operated

before the distributed capacitance starts becoming dominant. With the calculated values of inductance and distributed capacitance, f_o is found to be 42.8 GHz.

Since the thickness of the metal is taken to be 20 microns, to compute the series resistance R_s as a DC resistance the following formula shown in Equation 3.11 is used.

$$R_s = l/\sigma_{Cu}(\frac{\pi d^2}{4}) = 2\pi R/\sigma_{Cu}(\frac{\pi d^2}{4}) \tag{3.11}$$

where

l is the length of the toroid,

d is the diameter of the via, and

R is the mean radius of the toroid.

The mean radius R has to be found from the equation for the inductance of the toroid.

The Q factor of the inductor is given by

$$Q = X_L/R_s = 2\pi f L/R_s. \tag{3.12}$$

For a rectangular cross section,

$$L = \frac{\mu_o \mu_r N^2 A_c}{l_c} = \frac{\mu_o \mu_r N^2 w_c h_c}{2\pi R} \tag{3.13}$$

For a 20 turn inductor with $w_c = 50$ μm and $h_c = 250$ μm the mean radius of the toroid is found to be

$$R = \frac{\mu_o \mu_r N^2 w_c h_c}{2\pi L} \tag{3.14}$$

The calculated value of R with the given values is $12.5\mu m$. Substituting it back in Equation 3.11 the series resistance R_s is found to be 4.3 mΩ.

At high frequencies the thickness of the metal strip need not be considered in the formula for inductance because of skin effect which causes most of the current to be on the surface of the metal. So it is not used to derive L.

3.4 Modeling the Inductor

As seen in Figure 3.3 due to the way in which the toroidal structure is built the inductor is essentially modelled as a one-port network. S_{11} is the input reflection co-

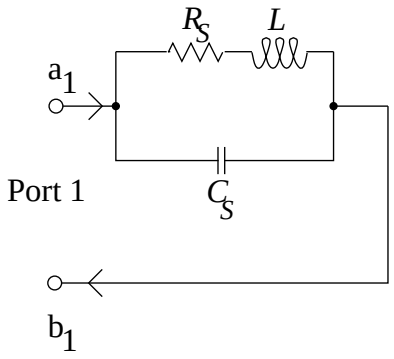

Figure 3.5: One port network model of the inductor.

efficient at port 1 which is used to calculate Z_{11}, the input impedance seen from port 1. Z_{11} is calculated using the formula for conversion from S-parameters to Z-parameters which is

$$Z_{11} = Z_o((1 + S_{11})/(1 - S_{11})). \tag{3.15}$$

where,

Z_o is the characteristic impedance of the port. This is normally 50 Ω.

3.5 Summary

So from discussions carried out so far the toroidal inductor is found to be compact and self-shielding. This structure requires fewer turns for a given inductance than does a solenoidal inductor. There is less ac resistance and the Q factor of the toroid can be increased dramatically.

Since the structure completely contains the magnetic flux within the material itself ideally no radiation occurs though practically some minimal radiation occurs. So there is very little loss due to radiation from the toroid and hence the Q factor does not reduce as much as it does in the solenoid.

Chapter 4

Results

4.1 Introduction

This chapter describes the simulations and experiments performed to realize the toroidal inductor structure. Comparisons are made between the results obtained from the simulations performed using Agilent's High Frequency Structure Simulator and measurements taken for the two fabricated structures.

4.2 Design goals

The design goals for the toroidal inductor include

- less area occupied on the package,
- high Q,
- high inductance; almost twice that of a solenoid-type inductor, and
- high self-resonant frequency so that the inductor can be operated over a wide band of frequencies.

The initial goal is to achieve good inductance in the range of 100 MHz to 1 GHz with low flux leakage for a higher Q factor. In the simulation and fabrication of the inductor the width of the metal strip at the top of the substrate is taken to be

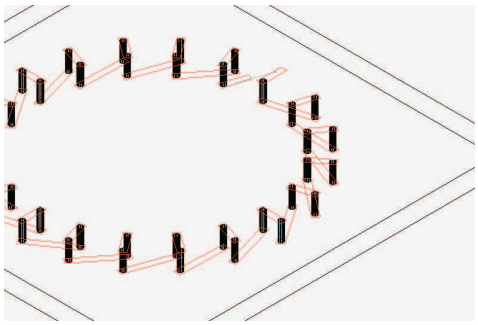

Figure 4.1: Isometric view of the toroidal inductor with unequal angles between each pair of top and bottom metal strips.

6 mm, the height of the substrate is 1.5 mm, the diameter of the via is 1.15 mm, the thickness of the metal strip is 20 microns, the mean radius of the toroid is 10 mm, the relative permittivity of the substrate is $\epsilon_r = 3.2$ and the relative permeability of the substrate is 1. The simulations have been carried out with a 20 turn toroidal inductors of the same dimensions as above.

4.3 Simulations

The toroid was simulated using Agilent's High Frequency Structure Simulator (HFSS). The metal strip was modeled as a thin metal in HFSS. Two new toroidal inductor structures were simulated with the aim of reducing flux leakage and reducing phase reversal of magnetic flux lines. The isometric views of the two structures are shown in Figures 4.1 and 4.2.

Figure 4.1 shows each pair of top and bottom metal strips placed at unequal angles with respect to each other. Figure 4.2 shows another way to construct the toroidal inductor structure.

In the simulation environment each of these structures is surrounded by an airbox 100 mm by 100 mm by 10 mm in size. In simulating these structures the airbox is assigned a radiation boundary condition. This boundary is also referred to as an absorbing boundary enabling you to model the surface as open. Therefore waves radiate outward, infinitely far into space. Because of the radiation boundary, the

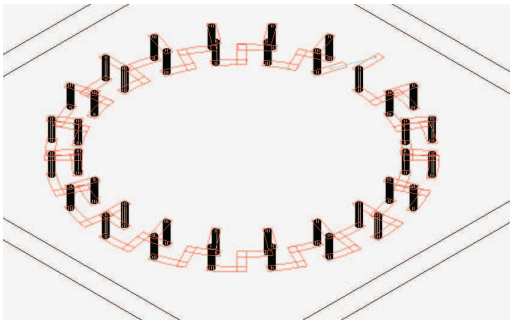

Figure 4.2: Another isometric view of the toroidal inductor with a different coil geometry.

calculated S-parameters include the effects of radiation loss.

Now consider the structure shown in Figure 4.1. The inductance (H) and Q factor versus frequency (Hz), magnitude and phase of S_{11} versus frequency (Hz) with the radiation boundary condition applied to the airbox are shown in Figures 4.3, 4.4, 4.5 and 4.6 respectively.

The inductance achieved with a radiation boundary is from 67 nH at 100 MHz to 0.2 μH at resonance. The resonant frequency is 900 MHz. With the radiation boundary condition the Q is down to around 36 which could be a more realistic figure since there will be some radiation from the structure into space. The radiation loss is incorporated in the Smith chart of Figure 4.7. The field plot shows that the magnetic flux lines are essentially completely inside the turns of the toroidal inductor with little or no radiation into space implying good flux linkage between the inductor turns.

Now consider the structure shown in Figure 4.2. The inductance (H) and Q factor versus frequency (Hz), magnitude and phase of S_{11} versus frequency (Hz) with the radiation boundary condition applied to the airbox are shown in Figures 4.9, 4.10, 4.14 and 4.14 respectively.

The inductance achieved with a radiation boundary is from 67 nH at 100 MHz to 0.26 μH at resonance. The resonant frequency is around 800 MHz. With the radiation boundary condition the Q is down to around 33 which could be a more realistic figure since there will be some radiation from the structure into space. The radiation loss is incorporated in the Smith chart of Figure 4.7. The field plot shows

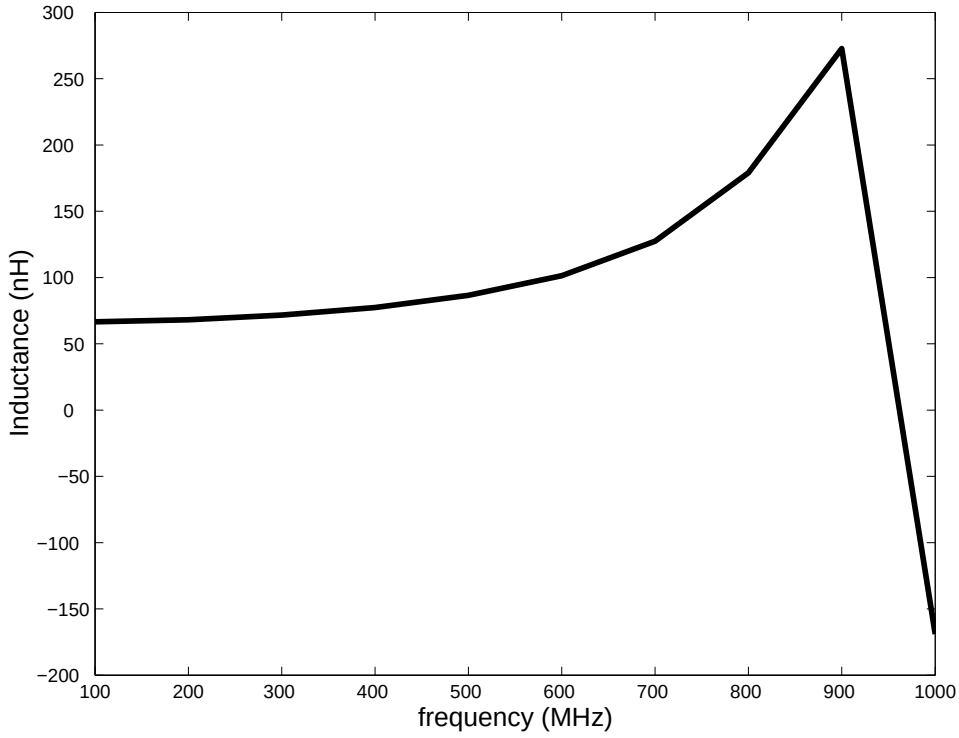

Figure 4.3: Inductance with the radiation boundary condition.

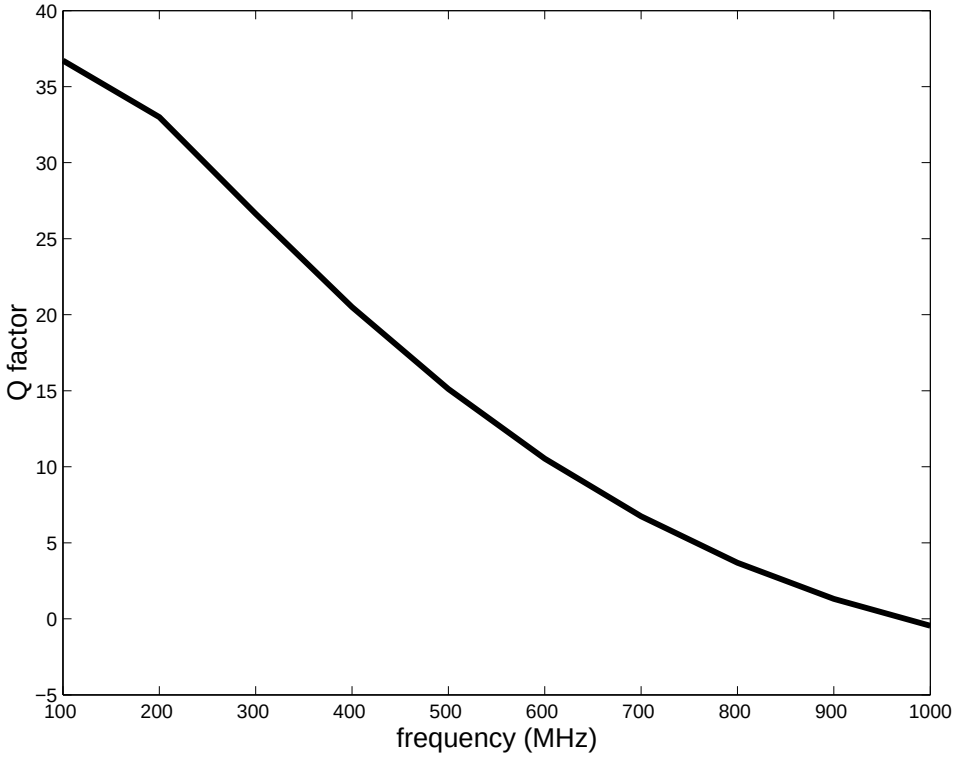

Figure 4.4: Q factor with the radiation boundary condition.

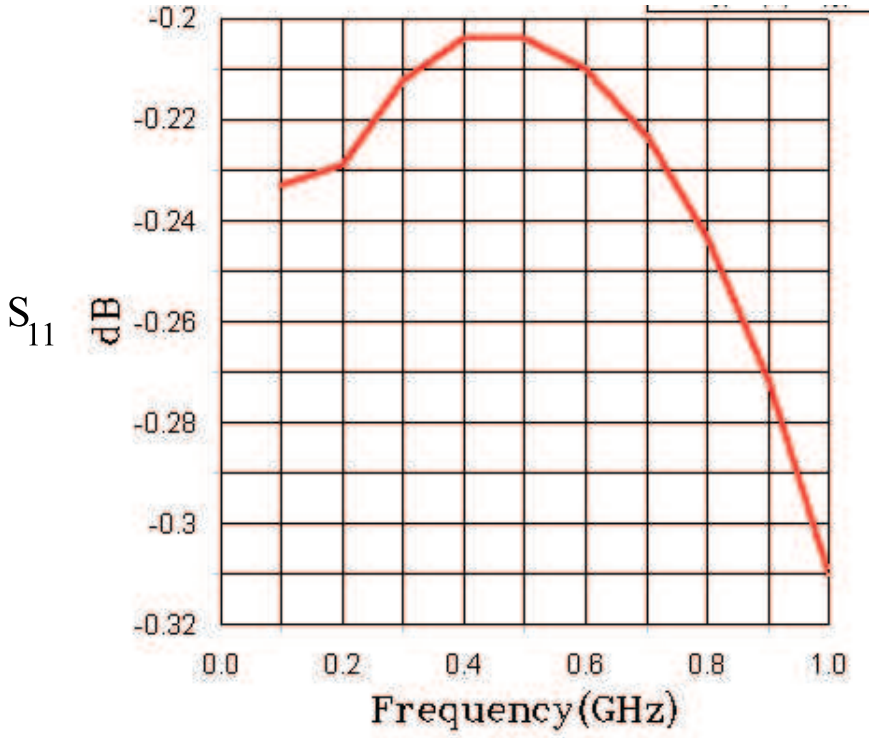

Figure 4.5: S_{11} magnitude with the radiation boundary condition.

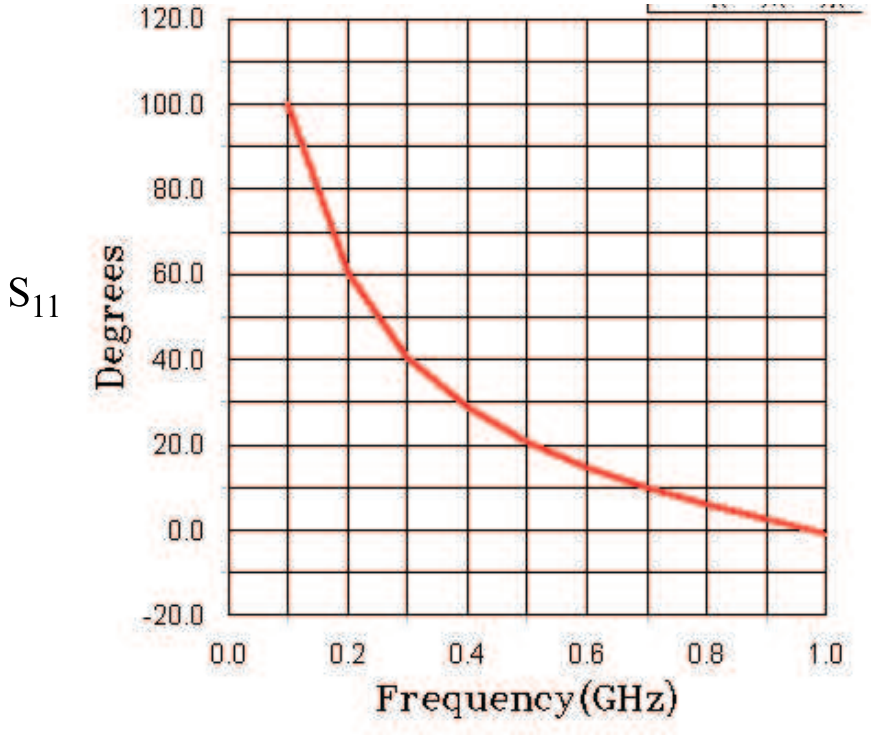

Figure 4.6: S_{11} phase with the radiation boundary condition.

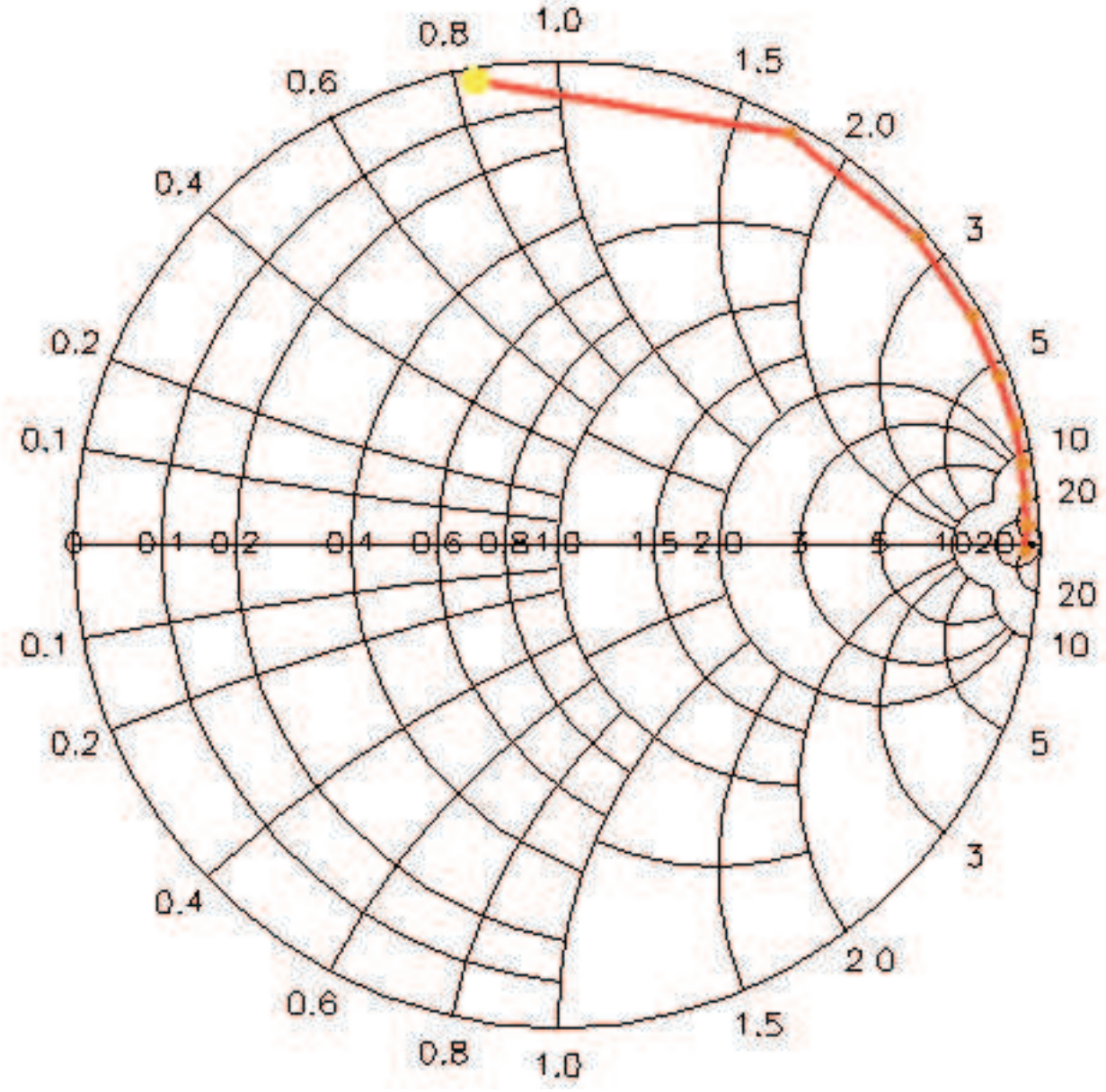

Figure 4.7: Smith chart showing the inductive nature of the structure from 100 MHz to 1 GHz for radiation boundary condition.

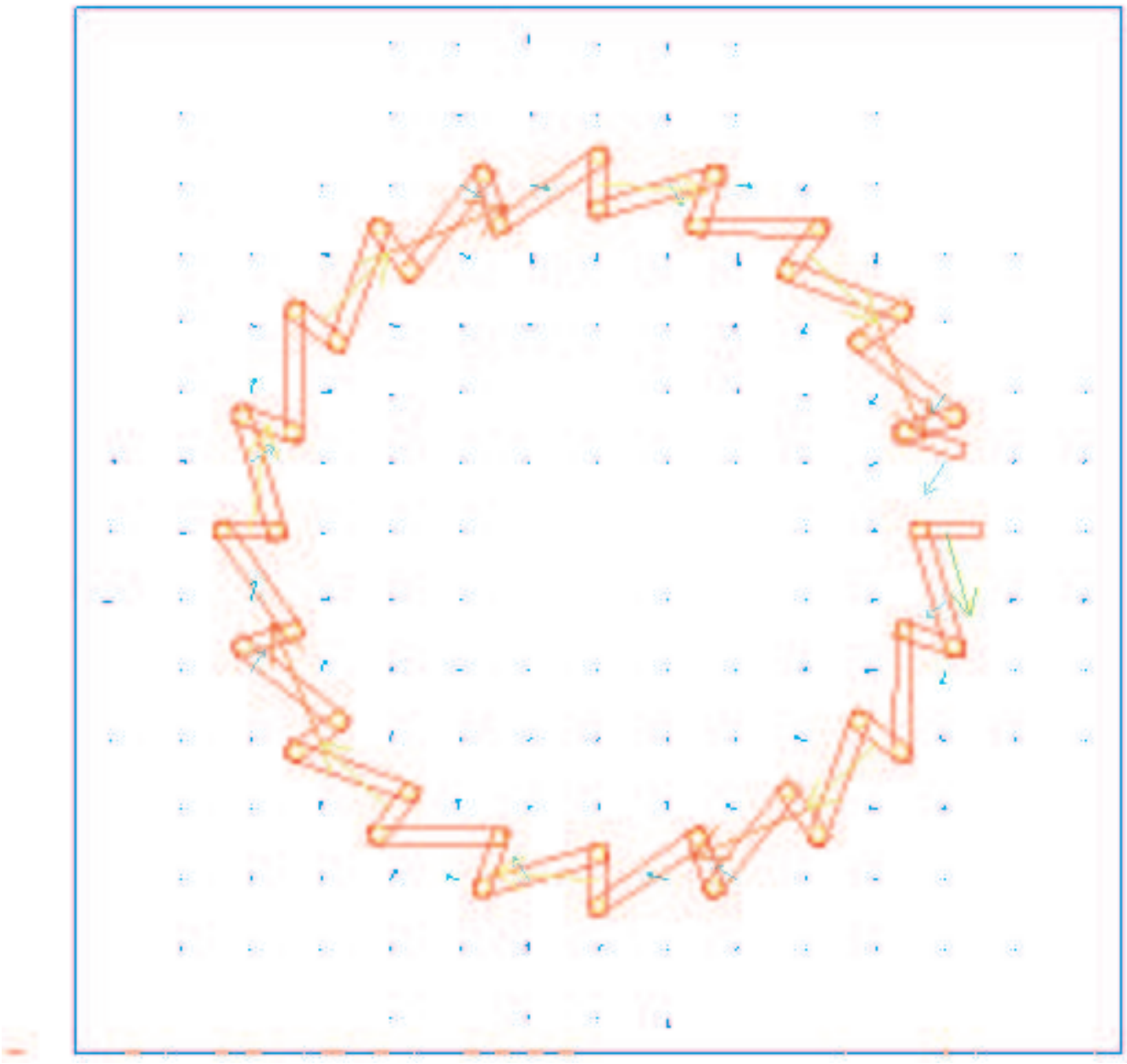

Figure 4.8: Plot of magnetic field in the XY plane for radiate boundary condition.

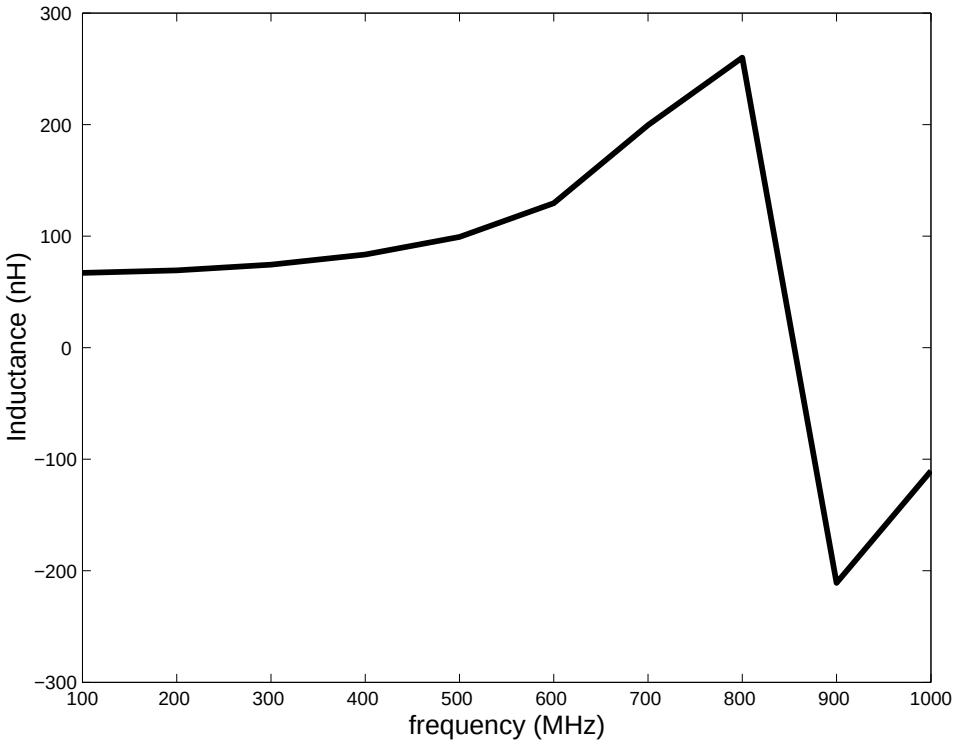

Figure 4.9: Inductance with the radiation boundary condition.

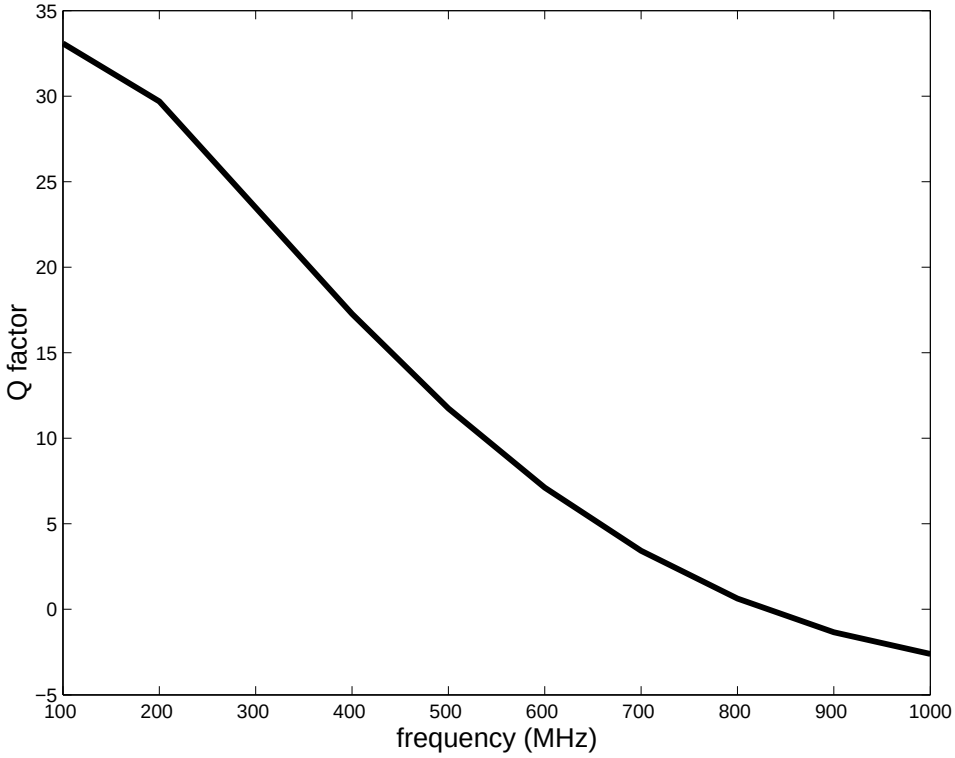

Figure 4.10: Q factor with the radiation boundary condition.

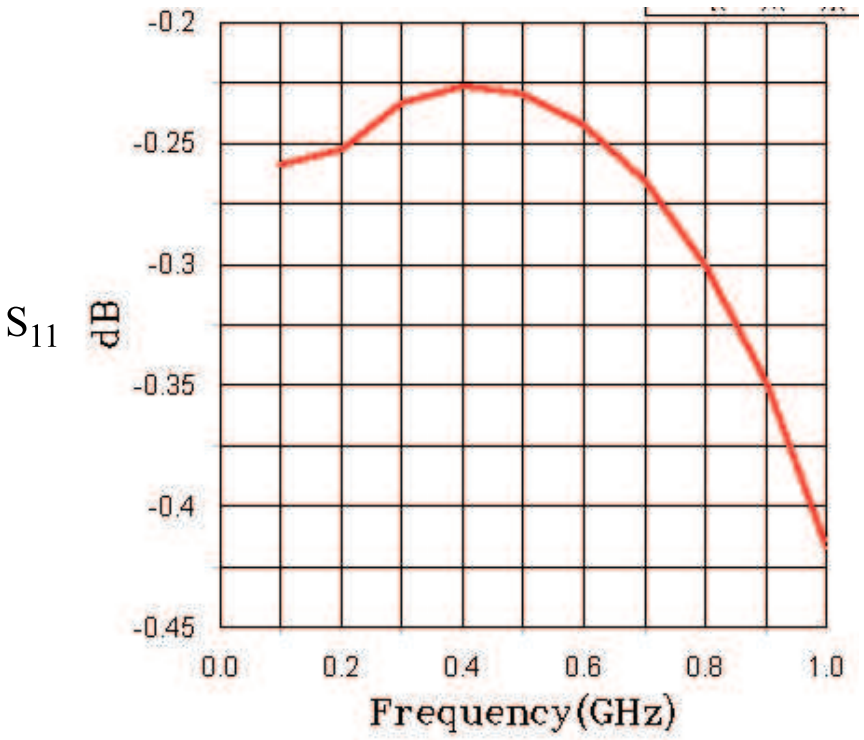

Figure 4.11: S_{11} magnitude with the radiation boundary condition.

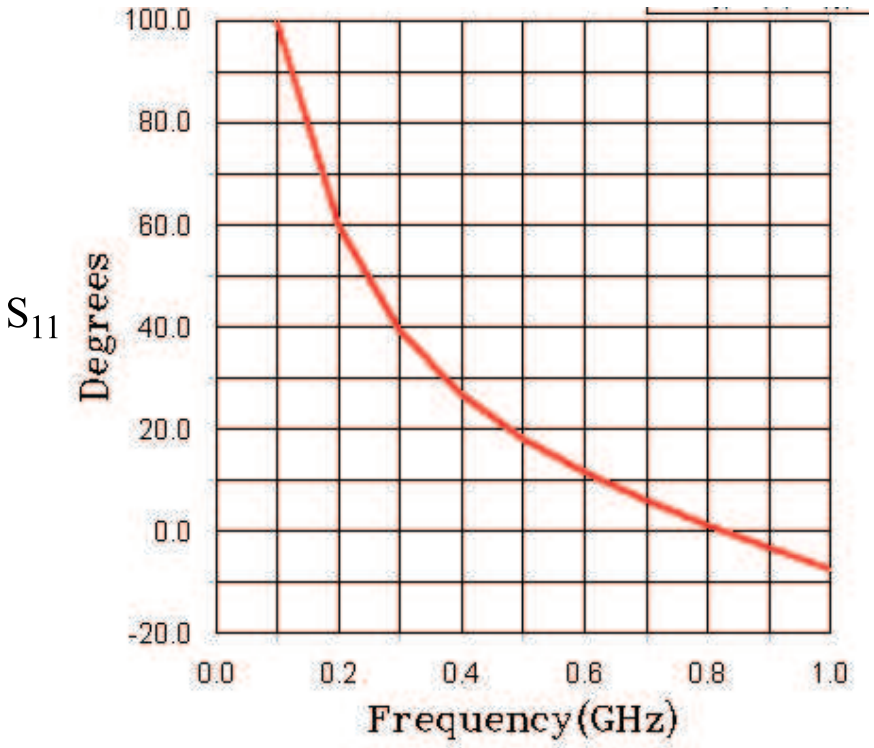

Figure 4.12: S_{11} phase with the radiation boundary condition.

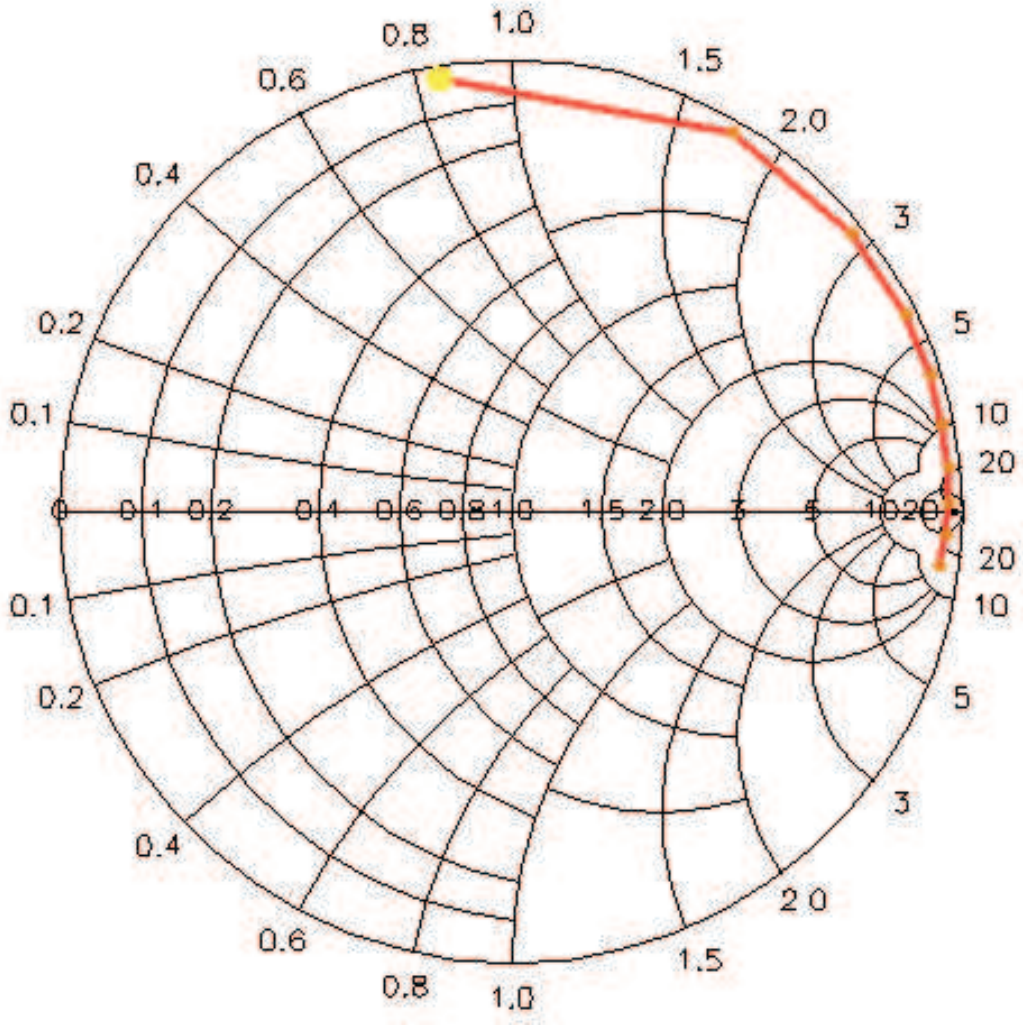

Figure 4.13: Smith chart showing the inductive nature of the structure from 100 MHz to 1 GHz for radiation boundary condition.

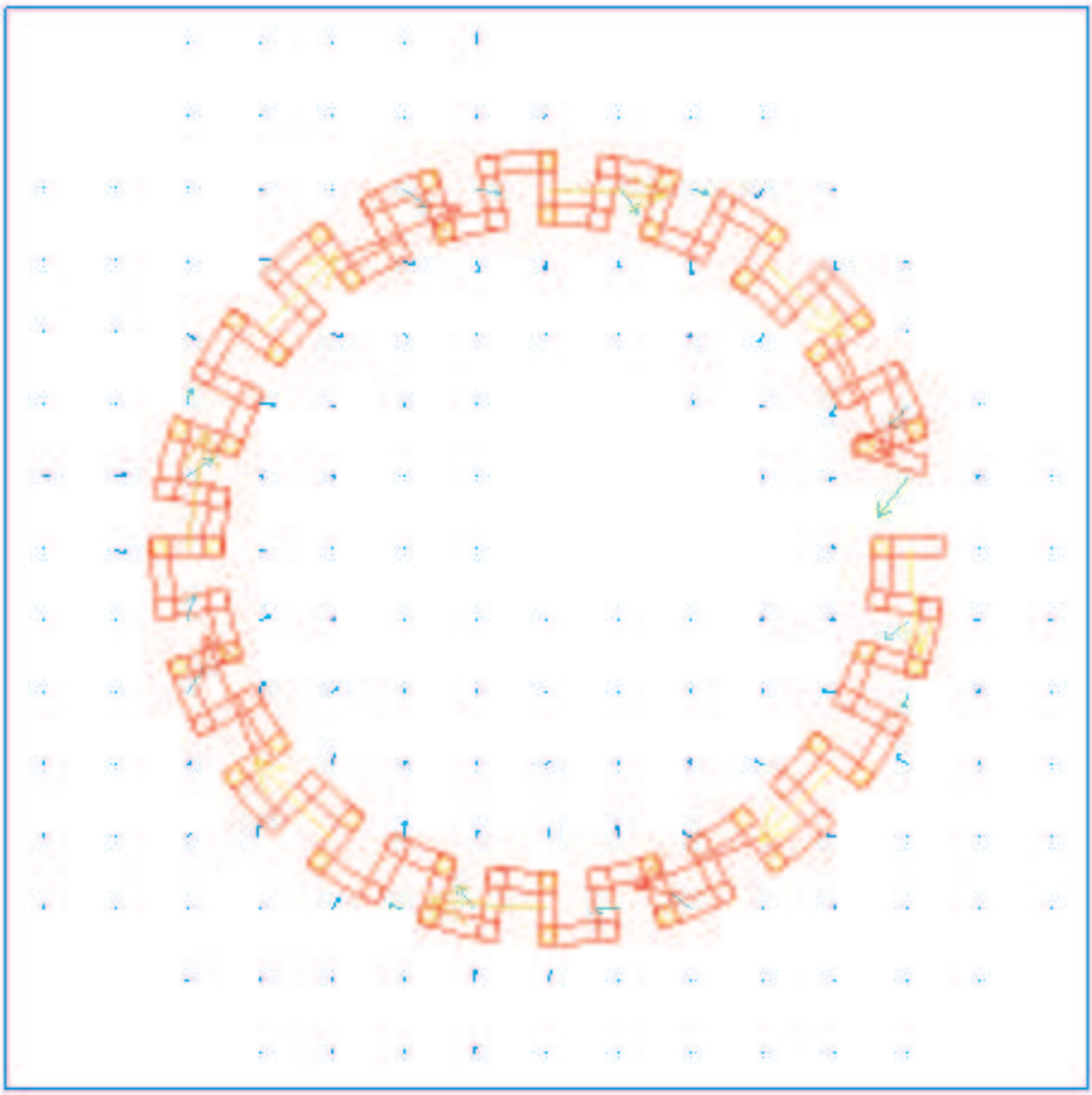

Figure 4.14: Plot of magnetic field in the XY plane for radiate boundary condition.

that the magnetic flux lines are essentially completely inside the turns of the toroidal inductor with little or no radiation into space implying good flux linkage between the inductor turns.

Comparing the two structures we find that the inductance offered by the structure shown in Figure 4.2 is higher than that offered by the other structure as frequency increases implying better flux linkage. Till about 600 MHz the two structures seem to offer the same inductance approximately. But the self-resonant frequency of the latter structure is less than that of the first one. This could simply be the effect of the latter structure being electrically longer than the previous one.

4.4 Calibration and Measurements

The direct measurement of the model parameters (inductance, resistance and stray capacitance) of the toroidal inductor is difficult because of the distributed nature and strong interaction of the parasitic effects. Typically, any of these parameters can only be obtained from measurable parameters such as impedance, quality factor and resonant frequency. We cannot ignore phase because of the frequency dependence of the model. Therefore, scalar (magnitude only) measurements are not adequate. Calibration structures are designed and fabricated on the same board as the inductor. The measurement is done using a Model 40A probe with Ground, Signal, Ground configuration and with 1250 microns pitch and the Vector Network Analyzer (HP 8510).

The calibration plane for the measurement of the S-parameters is at the probe tip. Error correction of the measured S-parameters involves calibration of the cable effects, connector mismatches, transmission line loss and phase compensation, up to the calibration plane. The SOLT (Short Open Load Thru) calibration procedure involves defining the standards precisely to the Network Analyzer (NA) in terms of what are known as calibration constants and performing a user calibration. The fabricated short and open structures are shown in Figure 4.16. The load was achieved by connecting a 50 Ω termination directly to the Network Analyzer cable and then performing the load calibration. The calibration structures have been fabricated in

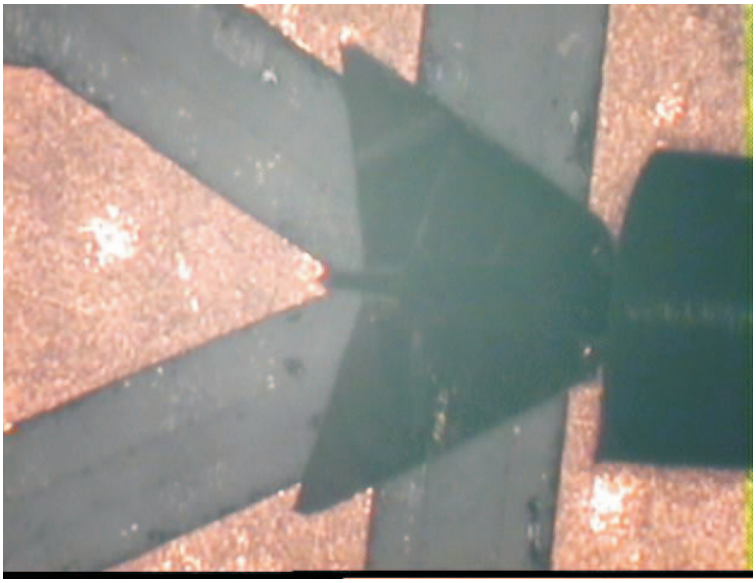

Figure 4.15: A snapshot of the 40A-GSG-1250-P Picoprobe.

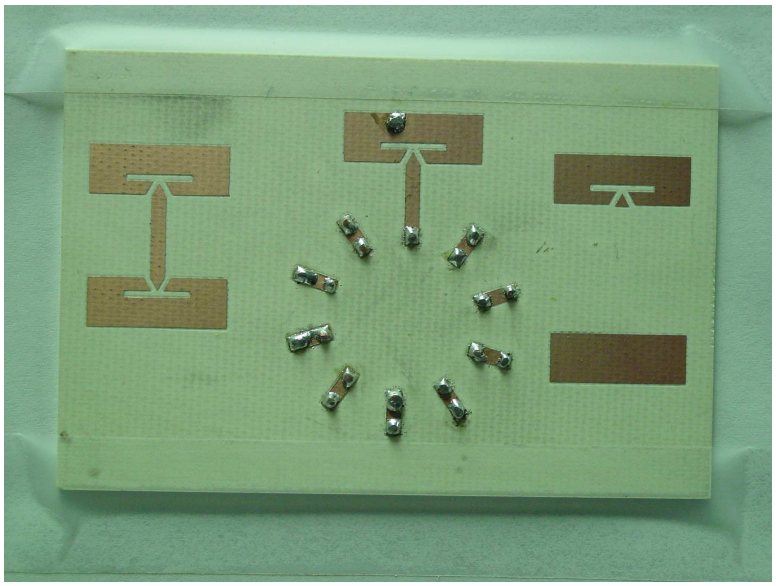

Figure 4.16: Fabricated short, open and load structures.

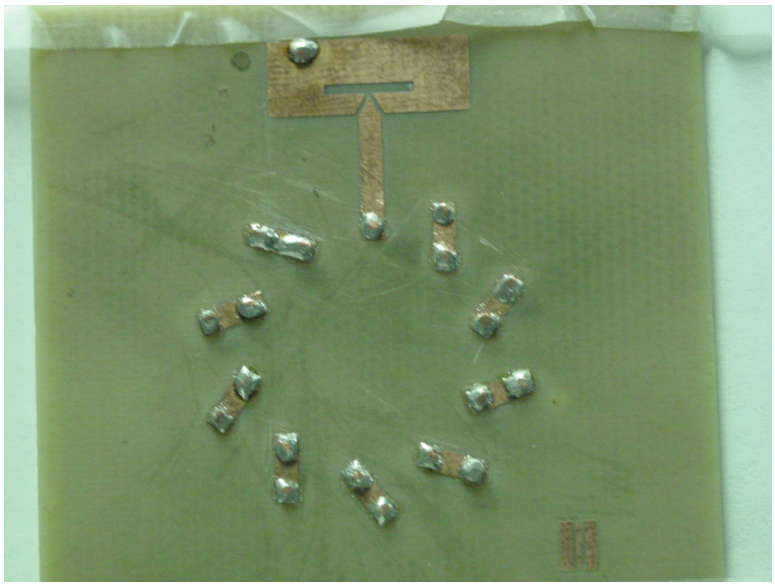

Figure 4.17: Top view of the toroidal structure with approximately equal angles between each pair of top and bottom metal strips.

the way shown in order to take care of the capacitance at the feed lines so that the effect it has on the measurement of the inductor is reduced.

The top and bottom views of the two structures fabricated are shown in Figures 4.17, 4.18, 4.19 and 4.20. The feed lines were designed to be 50Ω anywhere along the lines. This was done using Sonnet.

The comparison between the measured and simulated results for the first structure is shown below.

Looking at the smith chart in Figure 4.21 we see that the structure is inductive till around 700 MHz. The inductance achieved is from 84 nH at 100 MHz to 0.2 μH at resonance. The inductance achieved from the simulation in HFSS is from 83 nH at 100 MHz to 0.32 μH at resonance. The self-resonant frequency for the measurement is around 450 MHz. The inductance values obtained from the measurement and the simulation are quite comparable in Figure 4.22. The Q factor for the measurement is around 170 which is far beyond what is obtained from the simulation as can be seen in Figure 4.23.

The comparison between the measured and simulated results for the second struc-

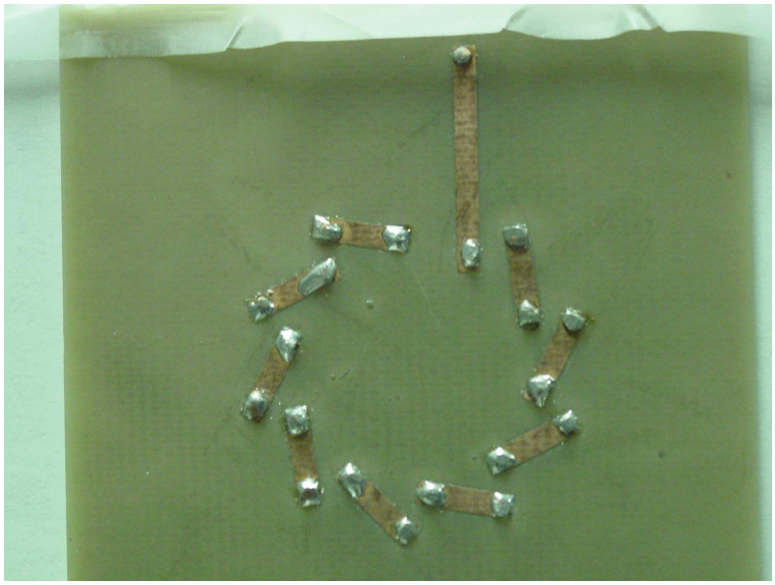

Figure 4.18: Bottom view of the toroidal structure with approximately equal angles between each pair of top and bottom metal strips.

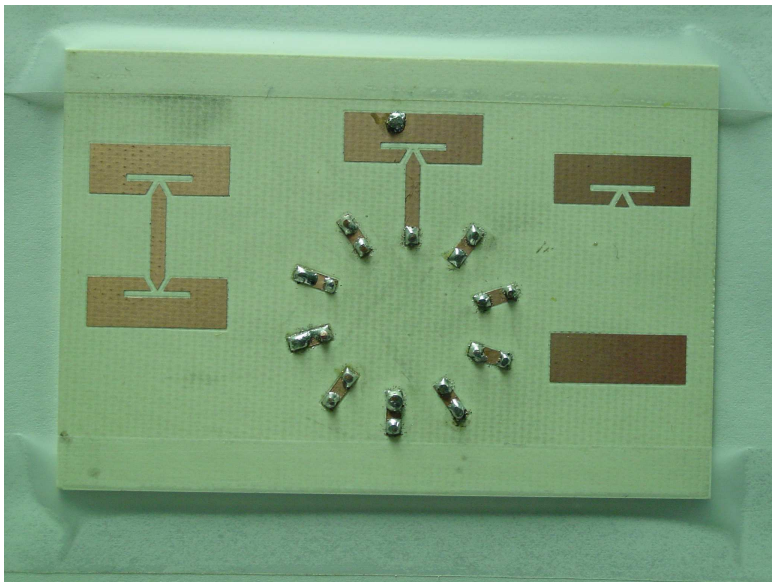

Figure 4.19: Top view of the second toroidal structure.

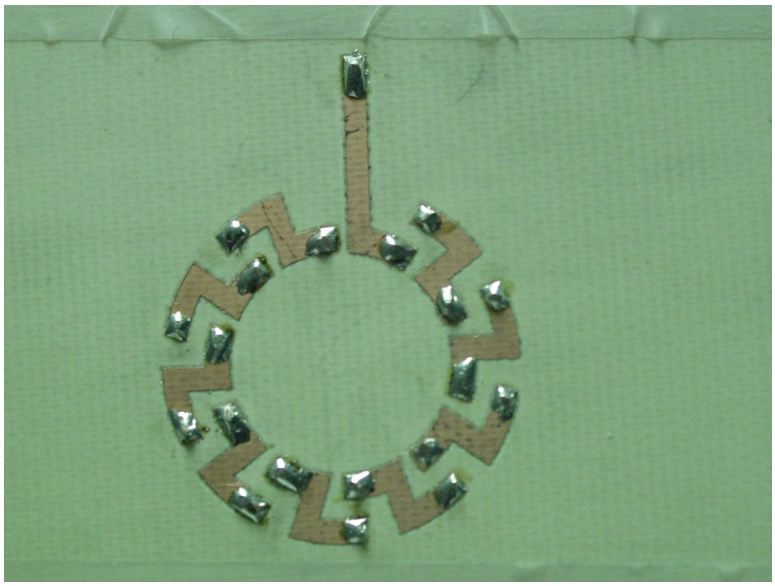

Figure 4.20: Bottom view of the second toroidal structure.

ture is shown below.

Looking at the smith chart in Figure 4.24 we see that the structure is inductive till around 500 MHz. The inductance achieved is from 93 nH at 100 MHz to 0.39 μH at resonance. The inductance achieved from the simulation in HFSS is from 80.4 nH at 100 MHz to 0.32 μH at resonance. The self-resonant frequency for the measurement is around 450 MHz. The inductance values obtained from the measurement and the simulation are quite comparable as seen in Figure 4.25. The Q factor for the measurement is around 150 which is far beyond what is obtained from the simulation as can be seen in Figure 4.26.

The working of the inductor was verified in many ways, for example by introducing a break in the metal strip. It was also verified using varying sizes of airbox around each of the three variations of the toroidal inductor. Different values of width of metal strip, different substrates (different values of dielectric constant), different metals for the metal strip, different number of turns keeping the mean radius of the toroid constant were some of the other techniques used.

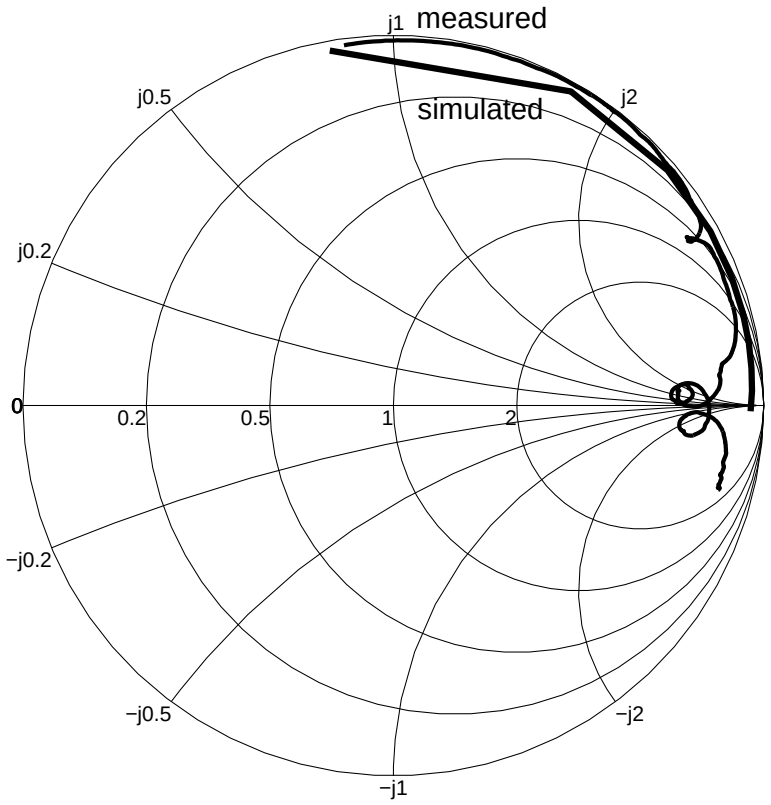

Figure 4.21: Smith Chart showing measured and simulated S_{11} for the first structure.

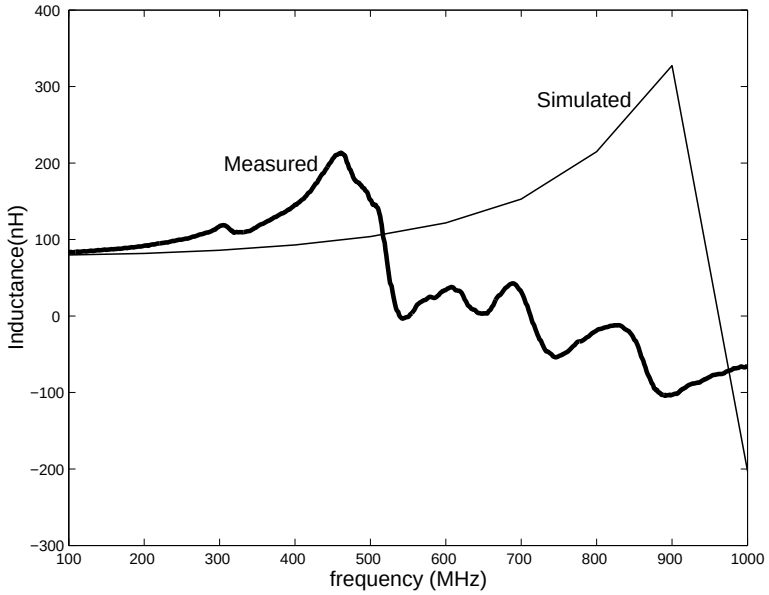

Figure 4.22: Comparison of the measured and simulated inductance values for the first toroidal inductor structure.

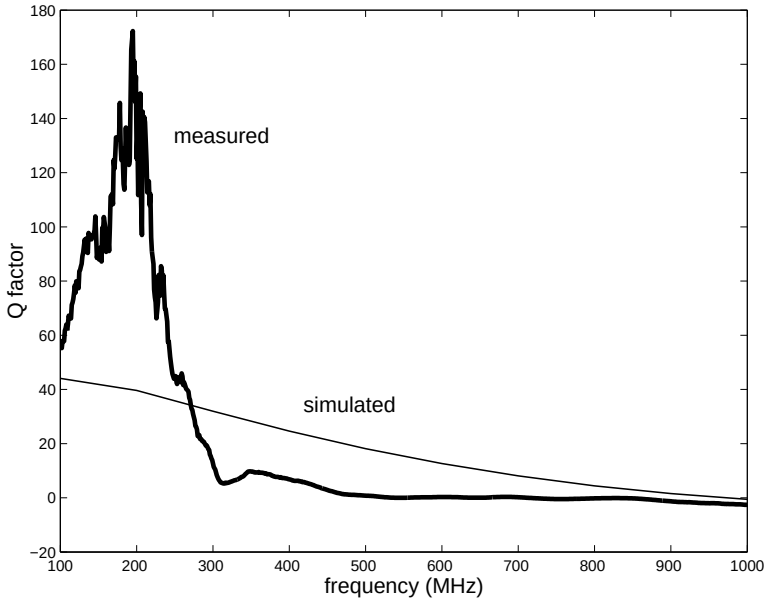

Figure 4.23: Comparison of the measured and simulated quality factor values for the first toroidal inductor structure.

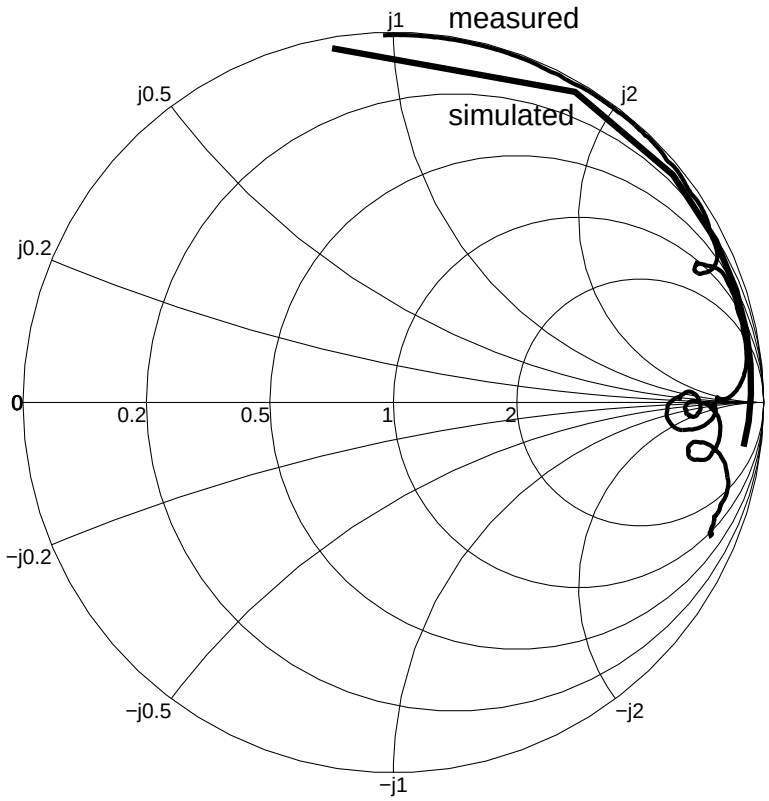

Figure 4.24: Smith Chart showing measured and simulated S_{11} for the second structure.

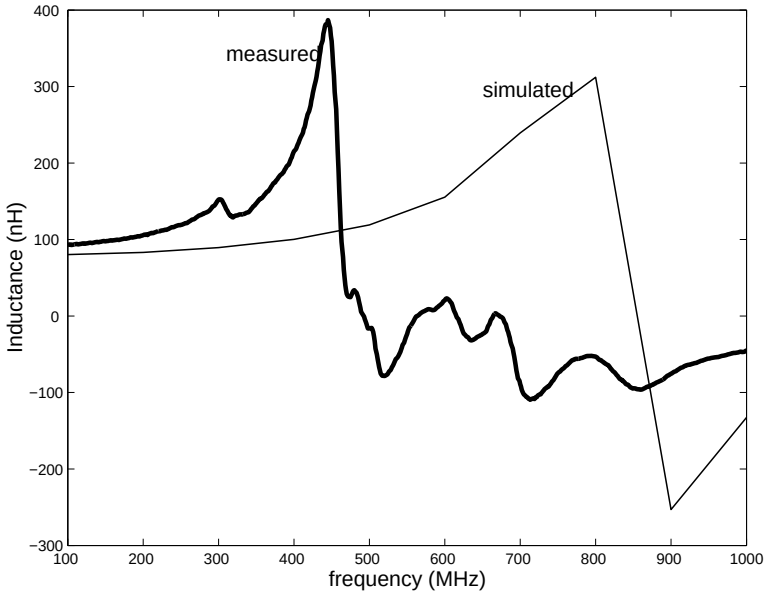

Figure 4.25: Comparison of the measured and simulated inductance values for the third toroidal inductor structure.

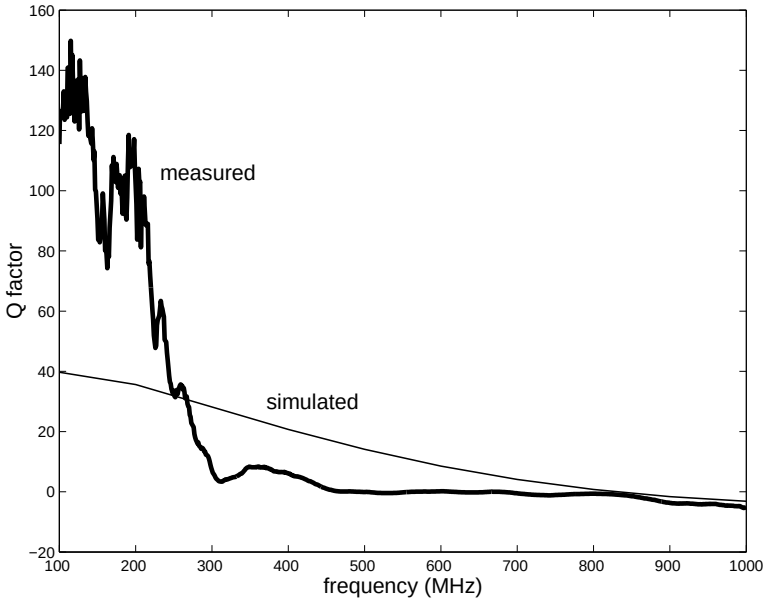

Figure 4.26: Comparison of the measured and simulated quality factor values for the third toroidal inductor structure.

Chapter 5

Conclusions

5.1 Conclusions

The toroidal inductor has been presented as a viable candidate for use in RF and microwave circuits on-chip or in-package. The structure has been simulated and measured in a frequency range of 100MHz to 1GHz. Two variations of the toroidal inductor have been simulated using Agilent's High Frequency Structure Simulator (HFSS) to study the effect of the placement of the top and bottom metal strips on the flux linkage and hence, the inductance and quality factor of the inductor.

In the first structure, each pair of top and bottom metal strips are placed at unequal angles with respect to each other. In the second structure, the top and bottom metal strips are placed uniformly around the circumference. A radiation boundary condition was applied to the airbox surrounding the toroid.

The simulation in HFSS yields a peak Q of 40 and a low frequency inductance of 0.8nH compared to a measured low frequency inductance of 0.9nH. The measured peak Q is very large, greater than 40, and the traditional reflection coefficient procedure cannot be used to determine a reliable value.

Both structures exhibit high inductance and high quality factor. The inductances of the two structures have been found to be comparable except at resonance where the inductance of the second structure becomes almost twice that of the first structure. The self-resonant frequency of the first structure (900MHz) is better than that of the

second structure (800MHz). The quality factor of the second structure is observed to be slightly lower than the first one. This could be simply because the second structure is electrically longer than the first one.

Three toroidal inductor structures have been fabricated and measured using the HP Vector Network Analyzer. The measurements indicate the self-resonant frequency for these structures to be around 400MHz.

Bibliography

[1] Simon Ramo, John R. Whinnery, Theodore Van Duzer, *Fields and Waves in Communication Electronics*, Wiley Publications, 1984.

[2] John D. Kraus, *Electromagnetics*, Mcgraw-Hill Publications, 1973.

[3] Reinhold Ludwig, Pavel Bretchko, *RF Circuit Design Theory and Applications*, Prentice-Hall Publications, 2000.

[4] Chris Bowick, *RF Circuit Design*, Newnes Publications, 2001.

[5] *HP High-Frequency Structure Simulator User's Reference.*

[6] Yeun-Ho Joung, Sebastien Nuttinck, Sang-Woong Yoon, Mark G. Allen, Joy Laskar, "Integrated Inductors in the Chip-to-Board Interconnect Layer Fabricated Using Solderless Electroplating Bonding," *2002 IEEE MTT-S Int. Microwave Symp. Dig.,* 2002.

[7] Yong-Jun Kim, Mark G. Allen, "Integrated Solenoid-Type Inductors for High Frequency Applications and Their Characteristics," *1998 IEEE Electronic Components and Technology Conf.,* Jun 1998.

[8] Krishna Naishadham, "Experimental Equivalent-Circuit Modeling of SMD Inductors for Printed Circuit Applications," *IEEE Trans. Electromagn. Compat.,* vol.43, Nov 2001, pp. 557–565.

[9] H.J.Ryu, S.D.Kim, J.J.Lee, J.Kim, S.H.Han, H.J.Kim, Chong H.Ahn, "2D and 3D Simulation of Toroidal Type Thin Film Inductors," *MMM-Intermag Conference,* Jan 1998.

[10] Martin O'Hara, "Modeling Non-Ideal Inductors in SPICE," *Newport Components, U.K.* Nov 1993.

[11] Seogoo Lee, Jongseong Choi, Gary S.May, Ilgu Yun, "Modeling and Analysis of 3-D Solenoid Embedded Inductors," *IEEE Trans. Electron. Packag. Manufacturing,* vol.25, Jan 2002, pp. 34–41.

[12] William B. Kuhn, Aaron W. Orsborn, Matthew C. Peterson, Shobak R. Kythakyapuzha, Aziza I. Hussein, Jun Zhang, Jianming Li, Eric A. Shumaker and Nandakumar C. Nair, "Spiral Inductor Performance in Deep-Submicron Bulk-CMOS with Copper Interconnects," *2002 IEEE Radio Frequency Integrated Circuits Symposium,* Aug 2002, pp. 385–388.

[13] Randall W. Rhea, "A Multimode High-Frequency Inductor Model," *Applied Microwave and Wireless,* Dec 1997.

[14] Bahl, I. J., "High current handing capacity multilayer inductors for RF and microwave circuits",' *Int. J. RF and Microwave Computer-Aided Engineering*, Vol. 10, No. 2, March 2000, pp. 139–146.

[15] Volant, R., Malinowski, J., Subbanna, S. and Begle, E., "Fabrication of high frequency passives on BiCMOS silicon substrates",' *2000 IEEE MTT-S Int. Microwave Symp. Dig.,* June 2000, pp. 209–212.

[16] Kuhn, W. B., "Approximate analytical modeling of currrent crowding effects in multi-turn spiral inductors," *2000 IEEE MTT-S Int. Microwave Symp. Dig.,* June 2000, pp. 405–408.

[17] Pun, A. L. L., Tau, J., Clement, J. R. and Su, D. K., "Substrate noise coupling through planar spiral inductor," *IEEE J. of Solid-State Circuits,* Vol. 33, June 1998, pp. 877–884.

[18] Kim, C. S., Park, M., Kim, C.-H., Park, M.-Y., Kim S.-D., Youn, Y.-S., Park, J.-W., Han, S.-H., Yu, H. K. and Cho, H., "Design guide of coupling between

inductors and its effect on reverse isolation of a CMOS LNA," *2000 IEEE MTT-S Int. Microwave Symp. Dig.,* June 2000, pp. 225–228.